Biosensors and Bioelectronics 71 (2015) 171–178

Contents lists available at ScienceDirect

Biosensors and Bioelectronics

journal homepage: www.elsevier.com/locate/bios

Novel electrochemical dual-aptamer-based sandwich biosensor using molybdenum disulfide/carbon aerogel composites and Au nanoparticles for signal amplification

Lin-Xia Fang, Ke-Jing Huang*, Yang Liu

College of Chemistry and Chemical Engineering, Xinyang Normal University, Xinyang 464000, China

ARTICLE INFO

Article history:
Received 8 January 2015
Received in revised form
4 April 2015
Accepted 12 April 2015
Available online 13 April 2015

Keywords:
MoS_2/carbon aerogel composites
Au nanoparticles
Platelet-derived growth factor BB
Sandwich assay
Signal amplification

ABSTRACT

A new electrochemical aptamer biosensor for the platelet-derived growth factor BB (PDGF-BB) detection has been developed based on the signal amplification of MoS_2/carbon aerogel composites (MoS_2/CA) and sandwich assay. A facile hydrothermal route assisted by L-cysteine was applied to synthesize CA incorporated flower-like MoS_2 with the large surface active sites and good conductivity. The electrochemical aptasensor was constructed by sandwiching the PDGF-BB between a glassy carbon electrode modified with thiol-terminated PDGF-BB aptamer-1 (Apt1)/gold nanoparticles (AuNPs)/MoS_2/CA and the AuNPs with thiol-terminated PDGF-BB aptamer-2 (Apt2) and 6-ferrocenyl hexanethiol (Fc). Fc–AuNPs–Apt2 acted as tracer and AuNPs/MoS_2/CA were utilized as the biosensor platform to immobilize a large amount of capture aptamers, owing to their layered structure and high surface-to-volume ratio. Based on the sandwich format, a dual signal amplification strategy had been successfully developed with a wide linear response in the range of 0.001–10 nM and a limit of detection of 0.3 pM. The developed assay demonstrated good selectivity and high sensitivity, indicating potential applications in bioanalysis and biomedicine.

1. Introduction

Platelet derived growth factor (PDGF) has got great attention due to its important role in the regulation of cell growth and division (Kohler and Lipton, 1974). PDGF is composed of two disulfide-linked polypeptide chains (A and B) and occurs in three isoforms: PDGF-AA, PDGF-BB and PDGF-AB (Zhang et al., 2009). Among them, PDGF-BB is a cancer-related protein, which is known to be related to the cell transformation process and in tumor growth and progression. Furthermore, PDGF-BB has been considered as a good predictor for early deterioration of renal function in diabetic nephropathy (Pierce et al., 1995). Thus, rapid, sensitive and precise determination of PDGF-BB is of great significance for disease diagnosis and treatment.

For the detection of proteins, electrochemical assays are faster than conventional biochemical strategies because they usually require small detection volumes, reusability and ease of operation (Yang et al., 2014). That is, they are simple and inexpensive. But, an obstacle is that the PDGF-BB expresses very low level in biosamples and need to develop an ultrasensitive method. The specificity is another barrier for electrochemical detection of PDGF-BB in biosamples because of the complexity of the coexistences. Therefore, biomolecules, such as antibodies, have been widely used to modify electrode to detect PDGF-BB (Vasudev et al., 2013). However, antibody has been reported expensive, temperature-sensitive, irreversibly denatured and has a limited shelf life (Li et al., 2010).

Aptamers (Apts) are single-stranded DNA or RNA sequences with high affinity to a variety of targets, including small molecules, ions and proteins (Famulok et al., 2007). They have been widely used in analytical bioassay and drug design (Wu et al., 2011). Apts can be generated using a repetitive in vitro selection and partitioning technology, called systematic evolution of ligands by exponential enrichment (SELEX), against virtually any target molecule (Liu et al., 2009). Apts have been attractive as recognition elements due to their good chemical stability, structure feasibility, small size, high specificity, flexible design, and ease of chemical modification of aptamers (Bi et al., 2014). Especially, the affinities of Apts for their targets are reported to be comparable to, or even higher than most monoclonal antibodies (Bi et al., 2014). Typical dissociation constants for aptamer–target complexes have been found in the picomolar to low micromolar ranges (Kim and Gu, 2014). Recently, Apts have been applied in electrochemical biosensors for PDGF-BB detection. For example, Han et al. have

* Corresponding author.
E-mail address: kejinghuang@163.com (K.-J. Huang).

http://dx.doi.org/10.1016/j.bios.2015.04.031
0956-5663/

reported a new Apts-based sensor using multi-labeled functionalized C_{60} nanohybrid as tracing tag for PDGF-BB detection (Han et al., 2013). Bai et al. (2012) developed an electrochemical assay for PDGF and thrombin based on single-walled carbon nanotubes and multi-labeled graphene sheets.

In order to obtain low detection limit and high sensitivity for PDGF-BB detection, signal amplification is a good choice. Some signal amplification strategies have been applied in electrochemical sensor based on nanomaterials which possesses the large surface area and well conductivity (K.J. Huang et al., 2014; Zhu et al., 2014). The large effective surface area allows more biomolecules to be immobilized at or near the electrode surface, which reduces the distance for electron transfer between the biomolecule and nanomaterials. As a result, the charge transfer to the electrodes becomes easier. In addition, the strong interactions between the biomolecule and electrode surface enhance the surface density of the adsorbed analytes (Ren et al., 2015). Layered micro/nanostructures with ultrahigh surface area and surface permeability have increasingly attracted research attention for the application of electrochemical sensors (Chakrabarti et al., 2013; J. W. Huang et al., 2014). The layered structures would increase the effective reaction area, meanwhile decreasing the electron transfer and ion diffusion paths, which will lead to better electrochemical performance (Tai et al., 2012). Recently, transition metal dichalcogenides (such as MoS_2) as 2D layered nano-materials analogous to graphene attracted great attention due to their carrier mobility (Chen et al., 2013), optical (Yin et al., 2012), and catalytic properties (Voiry et al., 2013). In contrast to graphene, MoS_2 nanosheets can be facilely synthesized in large scale and directly dispersed in aqueous solution without the need of surfactants or oxidation treatment. Recently, the MoS_2 nanosheets growth on carbon-based material such as graphene sheets had been synthesized, and they exhibited more excellent electrochemical behavior, high electron conductivity and larger surface area (Das et al., 2012; Cunningham et al., 2012). Carbon aerogel (CA) is a kind of mesoporous carbon material with a three-dimensional network structure of carbon particles (Zhu et al., 2006). It has been recognized as a promising electrode material due to its high surface area and electrical conductivity (Lee et al., 2010). Moreover, gold nanoparticles (AuNPs) had also received more and more attraction in constructing sensors because of their superior electrical, catalytic properties and remarkable biocompatibility (Feng et al., 2012). Therefore, MoS_2/CA nanocomposite coupled with AuNPs would greatly accelerate the interface electron transfer of modified electrode and expand the applications of MoS_2/CA nanocomposite for constructing sensor.

In the current study, a simple approach was used to prepare CA incorporated layered MoS_2 nanoflowers by using a facile hydrothermal route. A novel electrochemical aptasensor was developed by sandwiching the PDGF-BB between a glassy carbon electrode modified with thiol-terminated PDGF-BB aptamer-1 (Apt1)/gold nanoparticles (AuNPs)/MoS_2/CA and the conjugates of 6-ferrocenyl hexanethiol (Fc)–AuNPs–thiol-terminated PDGF-BB aptamer-2 (Apt2). voltammetry was used as the detection approach and Fc labeled AuNPs as tracer. The performance characteristics of the developed aptasensor and potential merits for PDGF-BB detection were investigated in detail. The new aptasensor combined the inherent signal amplification of AuNPs/MoS_2/CA composite film and sandwich reaction amplification. Moreover, the electrochemical sensor exhibited high sensitivity and extraordinary specificity for PDGF-BB detection.

2. Experimental

2.1. Apparatus

Cyclic voltammetry (CV) and differential pulse voltammetry (DPV) measurements were carried out on a CHI 660E Electrochemical Workstation (Shanghai CH Instruments, China) with a conventional three-electrode system composed of saturated calomel electrode (SCE) as reference, platinum wire as auxiliary and modified GCE as working electrode. The scanning electron micrographs were taken with a scanning electron microscope (SEM, S-4800, Hitachi, Japan) at an acceleration voltage of 14 kV. The sizes of nanoparticles were measured by transmission electron microscopy (TEM, JEM 2100, Japan). Raman spectra experiments was performed on a Renishaw Raman system model 1000 spectrometer with a 200 mW argon-ion laser at an excitation wavelength of 514.5 nm. X-ray powder diffraction (XRD) pattern was measured on a Japan RigakuD/Maxr-A X-ray diffractometer.

2.2. Reagents and materials

Resorcinol, formaldehyde, $Na_2MoO_4 \cdot 2H_2O$, L-cysteine, Sodium borohydride, Hydrogen tetra chloroaurate (III) trihydrate, trisodium citrate, 6-ferrocenyl hexanethiol (Fc) were purchased from Shanghai Chemical Reagent Corporation (Shanghai, China). Platelet-derived growth factor-BB (PDGF-BB), bovine serum albumin (BSA), carcinoembryonic antigen (CEA), thrombin (Hb) and immunoglobulin G (IgG) were obtained from Pepro-Tech Inc. (USA). 0.1 M phosphate buffer solution (PBS, pH 7.0) was prepared with 0.1 M Na_2HPO_4 and NaH_2PO_4 and adjusted by 0.1 M H_3PO_4 or 0.1 M NaOH solutions. Oligonucleotides were synthesized and purified by Sangon (Shanghai, China). The sequences of these oligonucleotides used in this work are listed as follows (Liu et al., 2014; Zhang et al., 2015):

Apt1: 5′-SH-$(CH_2)_6$-TTT TTT TTT TCA GGC TAC GGC ACG TAG AGC ATC ACC ATG ATC CTG-3′;

Apt2: 5′-SH-$(CH_2)_6$-TTT TTT TTT TCA GGC TAC GGC ACG TAG AGC ATC ACC ATG ATC CTG-3′.

2.3. Preparation of AuNPs and Fc–AuNPs–Apt2 conjugates

The AuNPs were prepared according to the previous method (Jiang et al., 2008). 100 mL $HAuCl_4$ solution (0.01%) was boiled with vigorous stirring, and then 2.7 mL trisodium citrate solution (1%) was quickly added and stirred for 10 min at the boiling point. The obtained solution was centrifugated at 6000 rpm to remove excess ions and the precipitate was resuspended in water. The obtained colloid AuNPs were stored in brown glass bottles at 4 °C before use. The TEM images of AuNPs are presented in Fig. S1A.

The Fc–AuNPs–Apt2 conjugates were prepared according to the previous assay (Wang et al., 2003). Firstly, 100 μL hexane containing 5.0 mM Fc and 200 μL Apt2 was added to 500 μL colloid AuNPs solution and stirred for 24 h. The resultant modified AuNPs remained in the aqueous phase. The solution was centrifuged, and the hexane phase containing Fc was decanted. The AuNPs capped with Fc and Apt2 were thoroughly rinsed with 500 μL hexane, resuspended in 500 μL of 0.1 mol/L phosphate buffered saline (PBS, pH 7.0). Following centrifugation of the mixture to remove the supernatant, the resulting Fc capped AuNPs were washed and redispersed in 500 μL PBS and stored at 4 °C for further use. The TEM images and UV–vis absorption spectra of the Fc–AuNPs–Apt2 conjugates are presented in Figs. S1B and S2.

2.4. Preparation of MoS_2/carbon aerogel composites

CA was prepared as follows: a mixture of resorcinol and

formaldehyde (molar ratio: 1:2) was dissolved in water and stirred for 20 min. Subsequently, the pH value of the above solution was adjusted to 6.5 with concentrated ammonia. The mixture was then left undisturbed for one day at 85 °C to form a transparent orange red sol. After filtered and dried, an orange red solid was obtained. The black carbon aerogel was achieved after the orange red solid was carbonized in N_2 atmosphere at 650 °C for 15 h.

The MoS_2/CA composites were prepared as follows: 0.1 g CA was firstly dispersed in 50 mL water. 0.5 g $Na_2MoO_4 \cdot 2H_2O$ was then added and ultrasonic dispersed for 30 min. After adjusting the pH value to 6.5 with 0.1 M NaOH, 10 g L-cysteine was added. The resultant mixture was diluted with water to 80 mL and violently stirred for about 1 h. The mixture was then transferred into a 100 mL Teflon-lined stainless steel autoclave and heated at 180 °C for 48 h. After cooling naturally, the MoS_2/CA was collected by filtration, washed with distilled water and absolute ethanol for three times, and dried in vacuum at 60 °C for 24 h. For comparison, MoS_2 nanosheets were prepared without CA via the same route.

2.5. Preparation of aptasensor and electrochemical measurements

Prior to modification, the surface of GCE was polished with 0.5 and 0.05 μm alumina slurry, and then washed successively with ethanol and water. Chitosan has been widely used for constructing sensors due to its attractive properties including excellent film-forming ability, high permeability, good adhesion and nontoxicity. It also facilitates the electron transfer after its swelling in reaction mixture due to its hydrophilic nature. In addition, chitosan has the abundant amino groups and could provide active sites for further AuNPs immobilization. Herein, 0.5 mg MoS_2/CA was suspended in 1 mL chitosan aqueous solution (0.1%) containing 1% acetic acid and sonicated to obtain a homogeneous black solution. Subsequently, 8 μL the MoS_2/CA solution was dropped onto the pretreated GCE to increase the effective area of the electrode. Then the electrode was dried at room temperature and exposed to AuNPs solution for 12 h following with rinsed with water and then dried. Subsequently, the formed AuNPs/MoS_2/CA

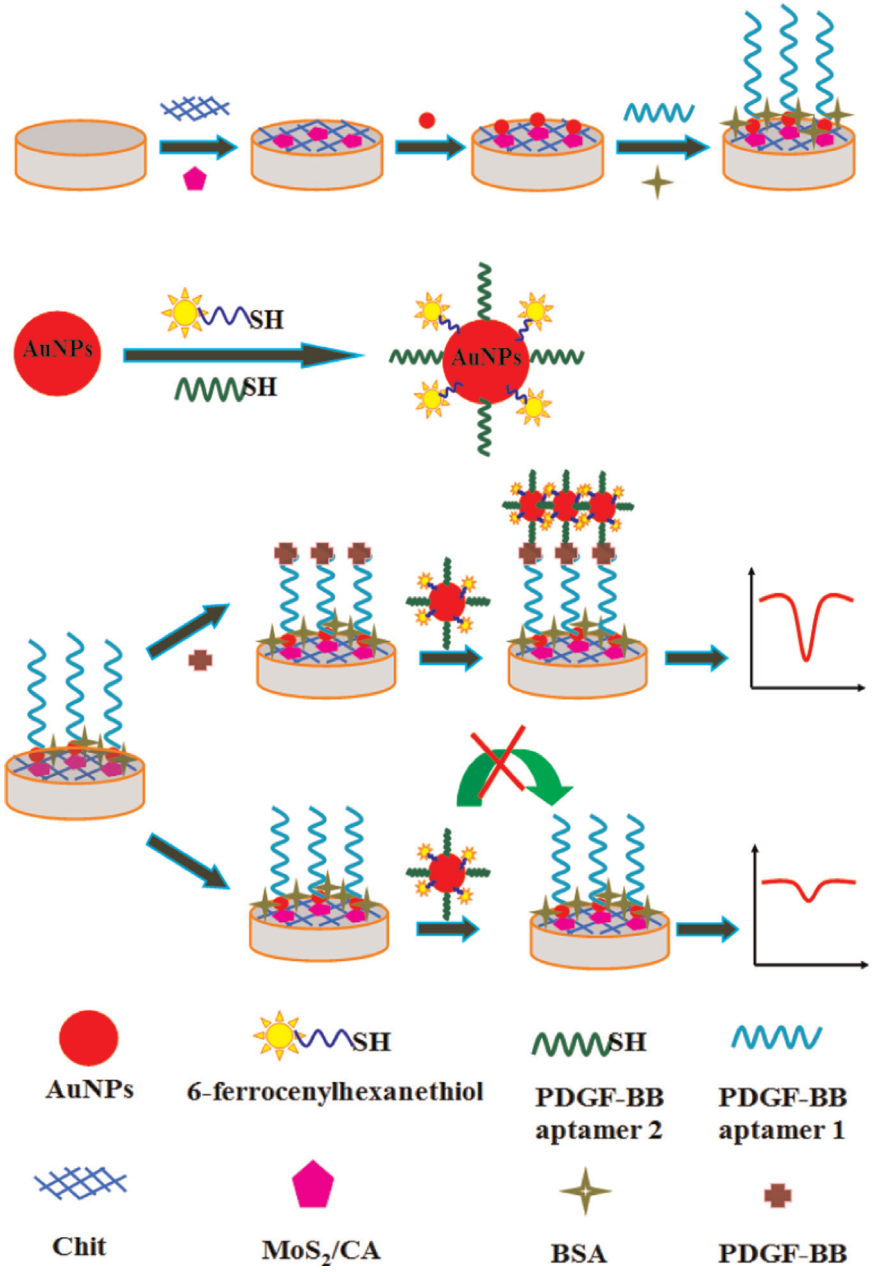

Scheme 1. Schematic diagram of the electrochemical aptamer biosensor based on AuNPs and MoS_2/CA signal amplification for the detection of PDGF-BB.

modified electrode was submerged into the 50 μL of 1 μM Apt1 solution for 3 h at room temperature. Then the resulting aptasensor was incubated with blocking solution (BSA, w/w, 0.25%) for 2 h to eliminate non-specific binding effects and block the remaining active groups. After every step, the electrode was thoroughly cleaned with PBS buffer and double distilled water to prevent the non-chemisorption. Next, this electrode was immersed in PBGF-BB solution for 2 h, rinsed with PBS to remove the nonspecifically bound PBGF-BB, and was then immediately soaked in 50 μL Fc–AuNPs–Apt2 conjugates for another 2 h. The whole process for the aptasensor preparation is illustrated in Scheme 1.

The electrochemical measurements were performed by cyclic voltammetry (CV) and the differential pulse voltammetry (DPV) in a 1.0 mM $[Fe(CN)_6]^{3-/4-}$ containing 0.1 M KCl. The instrumental parameters of DPV measurements were as follows: 0.005 V of pulse amplitude, 0.05 s of pulse width and 0.2 s of pulse period.

3. Results and discussion

3.1. Characterization of the as-prepared nanocomposites

The typical SEM image of as-prepared MoS_2 is shown in Fig. 1A. It exhibits many MoS_2 nanosheets stacked together. The thickness

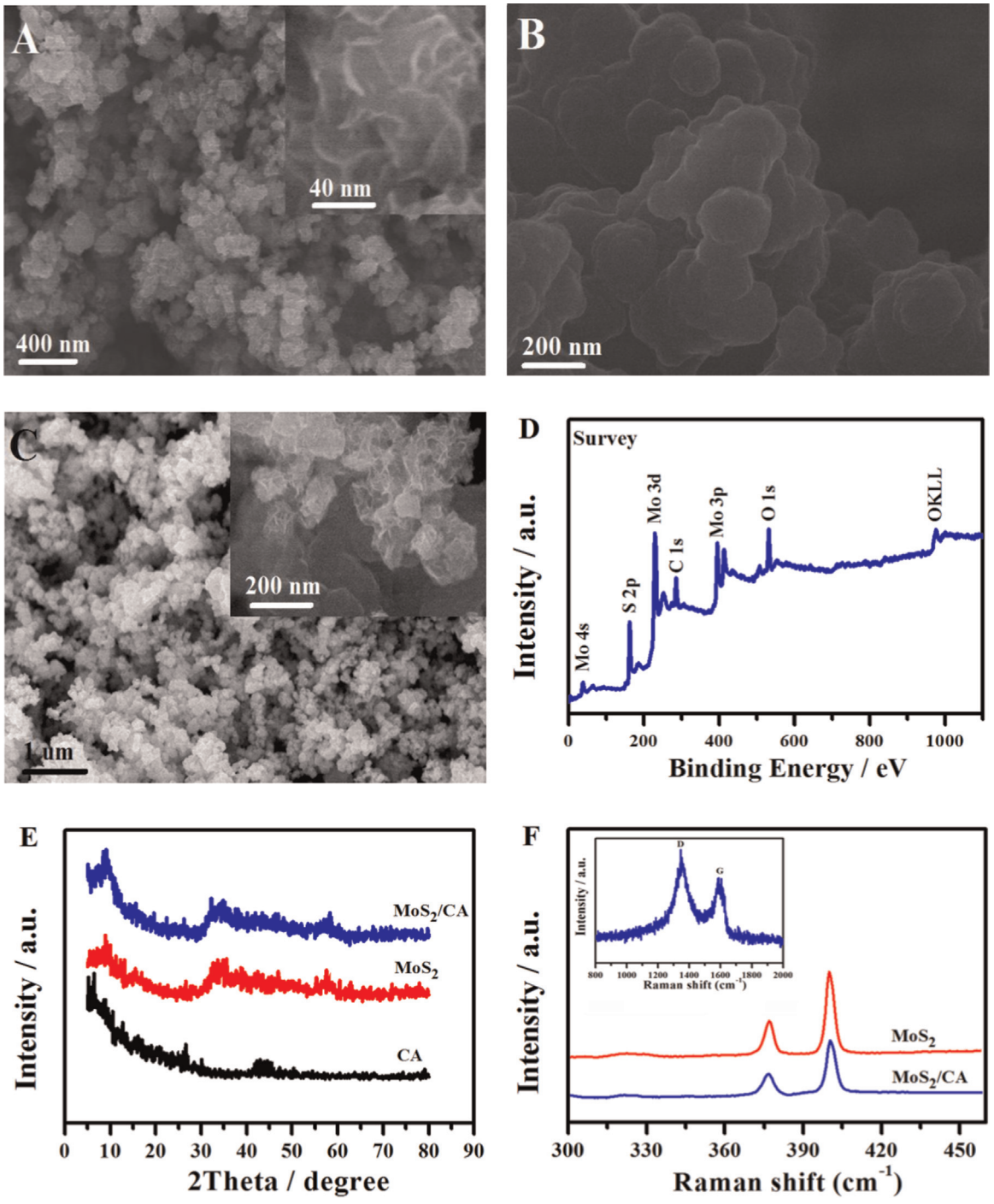

Fig. 1. SEM image of MoS_2 (A), AC (B) and MoS_2/CA composites (C); XPS survey spectra of MoS_2/CA composites (D); XRD patterns (E) and Raman patterns (F) of MoS_2, AC and MoS_2/CA composites.

of the nanosheet is several nanometers (inset of Fig. 1A). The SEM of CA is displayed in Fig. 1B. The pure CA nanoplates agglomerate together with average size of about 60 nm, resulting in non-uniformity dimension. Fig. 1C shows the MoS_2 nanosheets anchor on the CA plates, which is desirable for electrochemical biosensor application because both thin CA wafers and MoS_2 nanosheets are effective in improving the specific surface area and forming interconnected conducting network, which facilitates rapid electronic transport in electrode reactions.

The as-prepared MoS_2/CA composites were further characterized by XPS to verify their oxidation states and chemical composition. As shown in Fig. 1D, the predominant elements in the MoS_2/CA composites are Mo, S, C and O, and the atomic ratio of Mo to S is about 12. It has been reported that the electrons of the S atom layer and its adjacent carbon layer in the nanocomposites could form a coelectron cloud (Chang and Chen, 2011), and the high

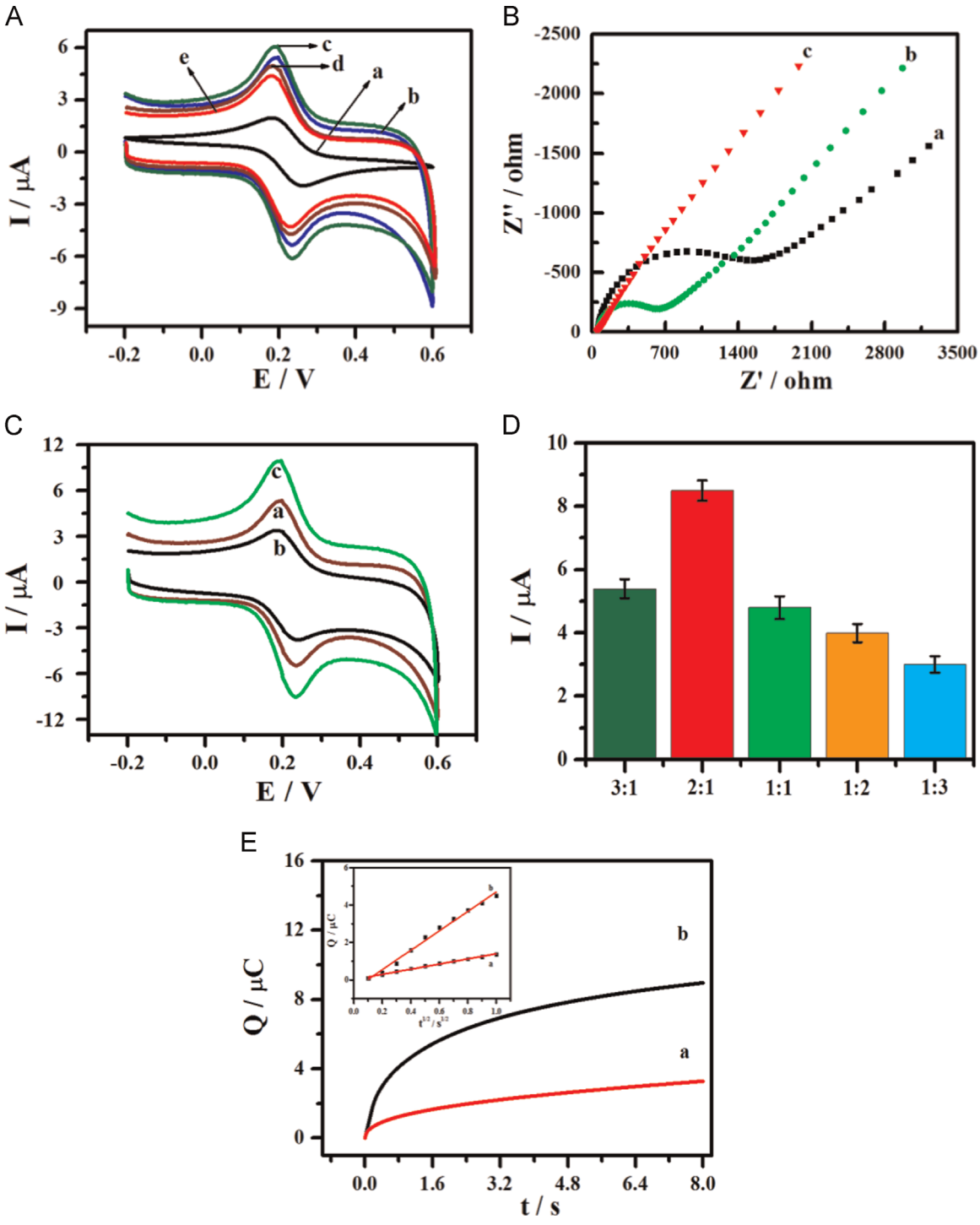

Fig. 2. (A) CV of different electrodes at a scan rate of 50 mV s^{-1}: (a) GCE, (b) MoS_2/CA/GCE, (c) AuNPs/MoS_2/CA/GCE, (d) Apt1/AuNPs//MoS_2/CA/GCE, (e) BSA/Apt1/AuNPs//MoS_2/CA/GCE; (B) Nyquist plots of bare GCE (a), MoS_2/CA/GCE (b), AuNPs/MoS_2/CA/GC (c); (C) CV of BSA/Apt1/AuNPs//MoS_2/CA/GCE (a), PGDF-BB/BSA/Apt1/AuNPs//MoS_2/CA/GCE (b), Fc–AuNPs–Apt2/PGDF-BB/BSA/Apt1/AuNPs//MoS_2/CA/GCE (c); (D) DPV response to the different volume proportions of AuNPs modified Fc (5 mM) and Apt2 (1 μM); (E) plot of Q–t curves of the (a) GCE and (b) AuNPs//MoS_2/CA/GCE. Inset: plot of Q–$t^{1/2}$ curves on (a) GCE and (b) AuNPs//MoS_2/CA/GCE. All the experiments were performed in 1.0 mM $[Fe(CN)_6]^{3-/4-}$ containing 0.1 M KCl.

concentration of electrons between the MoS_2 layer and the carbon layer could greatly enhance the electronic conductivity of the nanocomposites, which is beneficial to the transfer of ions and electrons diffusion during the electrode reaction.

The XRD diffraction patterns of CA, MoS_2 and MoS_2/CA composites are presented in Fig. 1E. The CA exhibits two broadened bands at 26° and 44° (2θ) which are attributed to (002) and (101) reflections of graphite carbon, showing the diffraction characteristics of graphite-like materials. The diffraction peaks of the MoS_2 sample show at $2\theta=14°$, 34°, 40° and 58°, which are assigned to the (002), (100), (103), and (110) planes of MoS_2 (JCPDS no. 37-1492), respectively. For the MoS_2/CA composites, the diffraction peaks of CA are rather weak because of the minor amount of CA present in the composite. However, one can still identify two diffraction peaks of CA and four diffraction peaks of MoS_2, which confirms the successful preparation of MoS_2/CA composites.

Fig. 1F shows the Raman spectrum of MoS_2/CA composites. Both MoS_2 and MoS_2/CA composites exhibit the characteristic bands at 379 and 404 cm^{-1}, corresponding to the A_{1g} and E_{2g} modes of the hexagonal MoS_2 crystal, respectively (Frey et al., 1999). In the higher wave number region (the inset in Fig. 1F), two Raman peaks appear at around 1350 and 1590 cm^{-1}, which are corresponding to the D and G bands of CA, respectively.

3.2. Electrochemical characterization

Electrochemical characteristics of the as-developed biosensor was studied by CV. Fig. 2A shows CVs of different modified electrodes in 1.0 mM $[Fe(CN)_6]^{3-/4-}$ solution containing 0.1 M KCl at a scan rate of 50 mV s^{-1}. At the bare GCE, it exhibits a well-defined redox peak (curve a), corresponding to the reversible redox reaction of $[Fe(CN)_6]^{3-/4-}$. With the immobilization of MoS_2/CA on the GCE, the redox peak currents increase greatly as the MoS_2/CA film can enhance the effective electrochemical surface area to facilitate the electron transfer (curve b). When the AuNPs are adsorbed on MoS_2/CA film, the redox peak currents are further improved (curve c) because the AuNPs are similar to a conducting wire which makes the electron transfer easier. However, the peak currents decrease obviously after Apt1 is assembled on the AuNPs/MoS_2/CA/GCE (curve d) due to the capture aptamer can severely hinder the electron transfer of $[Fe(CN)_6]^{3-/4-}$. Subsequently, when the non-electroactive BSA is employed to block nonspecific sites, the peak currents further decrease (curve e).

The AuNPs/MoS_2/CA/GCE was studied by EIS using 0.1 mM $[Fe(CN)_6]^{3-/4-}$ redox as probe (Fig. 2B). It shows that the electron transfer resistance (R_{et}) for bare GCE (curve a) is 1575 Ω. When MoS_2/CA composite is modified on GCE (curve b), the R_{et} value dramatically decreases to 628 Ω, suggesting that MoS_2/CA film promotes the electron transfer and enhances the conductivity of the electrode. While the MoS_2/CA/GCE is further modified with AuNPs, the EIS of the AuNPs/MoS_2/CA/GCE (curve c) displayed an almost straight line in the Nyquist plot of impedance spectroscopy, indicating the promotion of AuNPs to the electron transfer of $[Fe(CN)_6]^{3-/4-}$.

Signal amplification is very important for successful development of ultrasensitive aptasensor. The signal amplification performance of the developed aptasensor is studied and the results are shown in Fig. 2C. After the BSA/Apt1/AuNPs//MoS_2/CA/GCE incubated with PDGF-BB, the CV response decrease owing to the fact that the formation of PDGF-BB on the electrode retards the electron transfer tunnel (curve a). The curve b shows the redox peak current of the aptasensor enhances greatly after the sandwich reaction between the BSA/Apt1/AuNPs//MoS_2/CA/GCE and Fc–AuNPs–Apt2. The result maybe attributed to the dual signal amplification process: the sandwich reaction introduced many AuNPs, which could greatly promote electron transfer; the sandwich reaction brought a lot of Fc on the electrode surface which could be further produce stable and greatly amplified signal.

The effective surface areas (A) of GCE and AuNPs//MoS_2/CA/GCE were compared by chronocoulometry in 1.0 mM $K_3[Fe(CN)_6]$ solution containing 0.1 M KCl, according to the equation: $Q=2nFAcD^{1/2}t^{1/2}/\pi^{1/2}+Q_{dl}+Q_{ads}$, where c, Q_{dl} and Q_{ads} are the concentration of substrate, double layer charge and Faradaic charge, respectively. Other symbols have their usual meanings. According to the experiment results as shown in Fig. 2E, A was calculated to be 0.077 cm^2 and 0.268 cm^2 for GCE and AuNPs//MoS_2/CA/GCE, respectively, indicating the effective surface area of electrode increased greatly after modification with AuNPs//MoS_2/CA/GCE film.

3.3. Optimization of experimental conditions

To obtain excellent analytical performance, the amount of MoS_2/CA composites used to modified electrode was optimized. The results showed that the peak current increased notably when the amount of MoS_2/CA suspension increased from 0 to 8 μL. However, when it exceeded 8 μL, the peak current conversely showed gradual decline. Therefore, 8 μL MoS_2/CA suspension was selected for the fabrication of the MoS_2/CA film-coated electrodes in this work.

The ratio of the volume of Fc (5 mM) and Apt2 (1 μM) was optimized. As shown in Fig. 2C, when the ratio is less than 2:1, the DPV signal obviously decreases due to the less amount of Fc on the AuNPs; when the ratio was greater than 2:1, the electrochemical signal also deceases because the less quantity of Apt2 affects the amount of AuNPs combined with the PGDF-BB. Therefore, the optimized volume proportion of AuNPs modified Fc (5 mM) and Apt2 (1 μM) was determined to be 2:1.

The amount of the Apt2 determined the efficiency with which the Apt2 binds to PGDF-BB, and would affect the electrochemical signal. The effect of amount of Apt2 (1 μM) on the DPV signal was evaluated. The results showed the signal intensity gradually increased with the increase of the amount of Apt2 and then leveled off when the amount of Apt2 was 50 μL. Therefore, the optimal amount of the Apt2 was 50 μL.

In the present study, aptamer probe (Apt2) acted as not only capture probe but also signaling probe. The assembly time of Apt2 directly influenced the stability and surface density of the aptamer probe. The DPV response of electrode for different assembly periods of Apt2 was evaluated. The experimental results showed that the DPV signal was relatively low when the aptamer probe was incubated for below 30 min since the Apt 2 was probably unstable under such short assembly time. The peak current increased with the augment of assembly time and tended to constant at about 2 h. When the assembly time increased unceasingly, no obvious change in peak current was observed. Therefore, the incubation time of 2 h was applied as the optimum time for self-assembly of aptamer probes in the subsequent experiments.

We found that changing the incubation time of the Apt1 modified electrode and Fc–AuNPs–Apt2 in PBGF-BB solution caused an obviously effect on the peak current. Therefore, the dependence of PBGF-BB incubation time on the peak current was studied. The results showed the current response increased with the increase of incubation time and almost leveled off after 2 h. So 2 h min was chosen as the incubation time for the detection of PBGF-BB.

3.4. Analytical performance of aptasensor

Under the optimization conditions, the performance of the present aptasensor was tested by detecting PBGF-BB standard

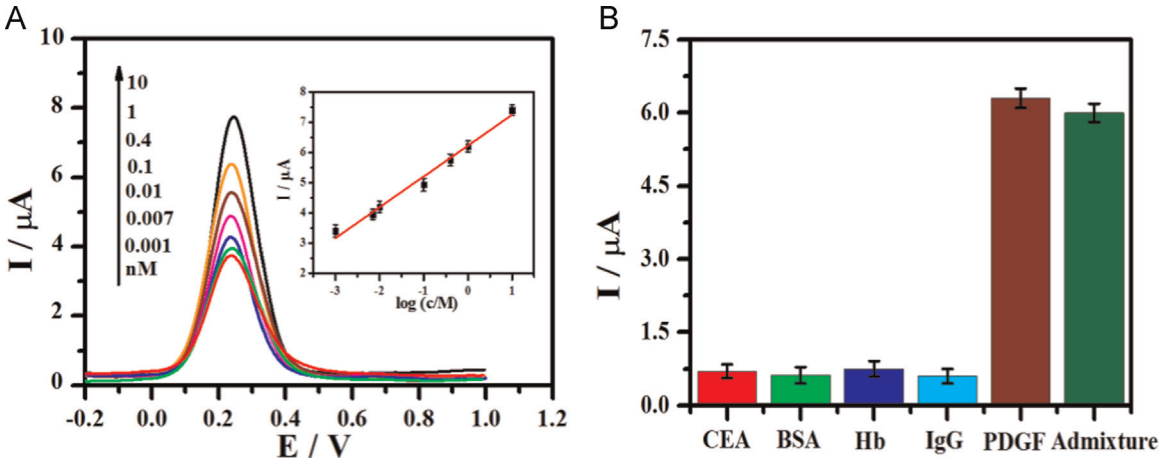

Fig. 3. (A) DPV responses of the proposed aptasensor after reaction with different concentration of PDGF-BB. *Inset*: The relationship of the peak current with log *c*; (B) Specificity of the aptasensor: BSA (1 μM), CEA (1 μM), Hb (1 μM), IgG (1 μM), PDGF-BB (1 nM), admixture of BSA (1 μM), CEA (1 μM), Hb (1 μM), IgG (1 μM), and PDGF-BB (1 nM). The error bars represent the standard deviations of three parallel samples at each target concentration.

solutions. Fig. 3A shows the typical DPV obtained after the sandwich reactions for different concentrations of PBGF-BB using Fc–AuNPs–Apt2 bioconjugates as tracer. As expected, the DPV responses increase with the increment of PBGF-BB concentrations. As shown in the inset of Fig. 3A, the calibration plots displays a good linear relationship between the peak currents and the PBGF-BB concentrations in the ranges of 0.001–10 nM with a regression equation of i (μA)=1.02 log(c/M)+6.23 (i is the peak current and c is the concentration of PBGF-BB) with a correlation coefficient (R) of 0.991. The detection limit was calculated to be 0.3 pM based on three times the standard deviation of the blank sample measurement. The analytical performance of proposed aptasensor is compared with other methods for PBGF-BB detection (Table 1). The proposed one is superior in wide linear range and low detection limit (Han et al., 2013; Bai et al., 2012; Wang et al., 2013, 2009; Ruslinda et al., 2012). The reason should be taken into account as the employment of the excellent electrical conductivity and biocompatibility of MoS_2/CA and the high-performance amperometric response of Fc–AuNPs–Apt2 which exhibited satisfactory performance as expected.

3.5. Specificity of the aptasensor

The specificity of the proposed biosensor played an important role in detecting biological samples in situ without separation. To evaluate the binding specificity of the developed aptasensor to PDGF-BB, control experiments were carried out by using BSA (1 μM), CEA (1 μM), Hb (1 μM) and IgG (1 μM) to replace 1 nM PDGF-BB, respectively. The results are shown in Fig. 3B. It is found that the presence of the interferences display no obvious effect on the peak current compared with the absence of PDGF-BB, indicating that the aptamer probe sequence is quite specific to PDGF-BB. Furthermore, the cross-sensitivity of the proposed aptasensor in a mixture solution (1 nM PDGF-BB containing 1 μM BSA, 1 μM CEA, 1 μM Hb and 1 μM IgG) is also investigated. Although high concentrations of these interferences are coexisted, the detection signals have no apparent difference, suggesting that the above interferents had almost negligible influence for PDGF-BB detection. The results demonstrate that the non-specific proteins do not interfere with PDGF-BB detection obviously. This excellent selectivity indicates that the developed biosensor holds promise in the detection of PDGF-BB in complex samples.

3.6. Repeatability and stability

The reproducibility of the developed aptasensor was tested. The peak currents of nine successive measurements of 0.1 nM PDGF-BB by DPV were performed and the relative standard deviation (RSD) of 1.9% was achieved. Five parallel-prepared BSA/Apt1/AuNPs//MoS_2/CA/GCEs were used to detect 0.1 nM PDGF-BB and the RSD of 4.9% was obtained, suggesting good reproducibility. Furthermore, the stability of the as-prepared aptasensor was investigated long-term storage assay. The rustled aptasensors were stored at 4 °C when they were not in use. The results showed that 96.3% of the initial response remained after one week and 90.1% of the initial response remained after one month, indicating the stability of the aptasensor was satisfactory. Meanwhile, thee results highlighted that AuNPs//MoS_2/CA as matrix had good stability and biocompatibility.

3.7. Application of the electrochemical aptasensor

To further validate the applicability of the proposed method, the contents of PDGF-BB in human serum samples collected from three healthy people were determined. 0.1 mL serum sample was added in 10 mL PBS (0.1 M) and then were detected with the aptasensor. As can be seen from Table 2, the value of PDGF-BB in two patients is much higher than that in three healthy persons. Table 2

Table 1
Comparison between different methods based on aptamer for PDGF-BB detection.

Analytical methods	Linear range (nM)	LOD (pM)	Ref.
Electrochemical sandwich sensor based on Multi-labeled functionalized C_{60} nanohybrid	0.002–40	0.6	Han et al. (2013)
Electrochemical sandwich sensor based on single-walled carbon nanotubes and multi-labeled graphene sheets	0.01–35	8	Bai et al. (2012)
Chemiluminescent sandwich sensor based on hydroxylamine amplified AuNPs	0.06–6	60	Wang et al. (2013)
Fluorescent sandwich sensor based on functionalized diamond surface	0.001–100	4	Ruslinda et al. (2012)
Electrochemical sandwich sensor based on AuNPs	0–0.001	0.01	Wang et al. (2009)
Electrochemical sandwich sensor based on AuNPs/MoS_2/CA	0.001–10	0.3	This work

Table 2
Determination of PDGF-BB in human serum samples by proposed electrochemical sensor and ELISA method ($n=3$).

Samples	Electrochemical sensor (average value ± SD)	ELISA	Relative deviation (%)
1	4.3 ± 0.1	4.2	2.4
2	5.4 ± 0.3	5.7	−5.3
3	4.8 ± 0.2	5.0	−4.0
4	14.3 ± 0.6	13.7	4.4
5	12.6 ± 0.5	13.1	−3.8

also shows that the target concentrations obtained by the proposed method are in good agreement with those determined by the ELISA method and the relative deviation are not more than 5.3%, indicating that it is feasible to apply the developed aptasensor to detecting PDGF-BB in human serum samples.

4. Conclusion

In summary, a novel sandwich electrochemical aptasensor for the sensitive detection of PGDF-BB has been developed by means of Apt2 and Fc labeled AuNPs as tracer. Carbon aerogel incorporated flower-like molybdenum disulfide was synthesized via a facile hydrothermal route assisted by L-cysteine and was applied to modified electrode to achieve excellent electrochemical performances. Highlights of this work can be concluded as follows: firstly, MoS_2/CA exhibited the large surface active sites and good conductivity. Secondly, AuNPs were not only used as an immobilization matrix but also help to increase conductivity of the composite film. Moreover, the Fc–AuNPs–Apt2 was a promising redox probe to generate high-performance amperometric response, thus greatly enhanced the detection signal for sandwich-type assay. Significantly, the large surface area, rich active sites, good conductivity and favorable microenvironment made the AuNPs/MoS_2/CA may become a promising nano-material for electrochemical aptasensing applications. Finally, we expected more exciting opportunities to explore MoS_2/CA-based new nanomaterials in future.

Acknowledgments

This work was supported by the National Natural Science Foundation of China (U1304214, 21475115) and Program for University Innovative Research Team of Henan (15IRTSTHN001).

Appendix A. Supplementary material

Supplementary data associated with this article can be found in the online version at http://dx.doi.org/10.1016/j.bios.2015.04.031.

References

Bai, L.J., Yuan, R., Chai, Y.Q., Zhuo, Y., Yuan, Y.L., Wang, Y., 2012. Biomaterials 33, 1090–1096.
Bi, S., Luo, B.Y., Ye, J.Y., Wang, Z.H., 2014. Biosens. Bioelectron. 62, 208–213.
Chakrabarti, M.H., Low, C.T.J., Brandon, N.P., Yufit, V., Hashim, M.A., Irfan, M.F., Akhtar, J., Ruiz-Trejo, E., Hussain, M.A., 2013. Electrochim. Acta 107, 425–440.
Chang, K., Chen, W.X., 2011. Chem. Commun. 47, 4252–4254.
Chen, J.R., Odenthal, P.M., Swartz, A., Floyd, G.C., Wen, H., Luo, K.Y., Kawakami, R.K., 2013. Nano Lett. 13, 3106–3110.
Cunningham, G., Lotya, M., McEvoy, N., Duesberg, G.S., Schoot, P.V.D., Cole-man, J.N., 2012. Nanoscale 4, 6260–6264.
Das, S.K., Mallavajula, R., Jayaprakash, N., Archer, L.A., 2012. J. Mater. Chem. 22, 12988–12992.
Famulok, M., Hartig, J.S., Mayer, G., 2007. Chem. Rev. 107, 3715–3743.
Feng, Q.L., Liu, K.P., Fu, J.J., Zhang, Y.Z., Zheng, Z.X., Wang, C.M., Du, Y.L., Ye, W.C., 2012. Electrochim. Acta 60, 304–308.
Frey, G.L., Tenne, R., Matthews, M.J., Dresselhaus, M.S., Dresselhaus, G., 1999. Phys. Rev. B: Condens. Matter Mater. Phys. 60, 2883–2892.
Han, J., Zhuo, Y., Chai, Y.Q., Yuan, R., Xiang, Y., Zhu, Q., Liao, N., 2013. Biosens. Bioelectron. 46, 74–79.
Huang, K.J., Liu, Y.J., Wang, H.B., Wang, Y.Y., Liu, Y.M., 2014. Biosens. Bioelectron. 55, 195–202.
Huang, J.W., He, Y.Q., Jin, J., Li, Y.R., Dong, Z.P., Li, R., 2014. Electrochim. Acta 136, 41–46.
Jiang, Y., Zhao, H., Zhu, N.N., Lin, Y.Q., Yu, P., Mao, L.Q., 2008. Angew. Chem. Int. Ed. 47, 8601–8604.
Kim, Y., Gu, M., 2014. Advances in Aptamer Screening and Small Molecule Aptasensors. Biosensors Based on Aptamers and Enzymes. Springer, Berlin, Heidelberg, pp. 29–67.
Kohler, N., Lipton, A., 1974. Exp. Cell Res. 87, 297–301.
Lee, Y.J., Jung, J.C., Yi, J., Baeck, S.H., Yoon, J.R., Song, I.K., 2010. Curr. Appl. Phys. 10, 682–686.
Li, D., Song, S., Fan, C., 2010. Acc. Chem. Res. 43, 631–641.
Liu, J., Cao, Z., Lu, Y., 2009. Chem. Rev. 109, 1948–1998.
Liu, Y.M., Zhou, M., Liu, Y.Y., Shi, G.F., Zhang, J.J., Cao, J.T., Huang, K.J., Chen, Y.H., 2014. RSC Adv. 4, 22888–22893.
Pierce, G.F., Tarpley, J.E., Tseng, J., Bready, J., Chang, D., Kenney, W.C., Rudolph, R., Robson, M.C., Berg, J.V., Reid, P., 1995. J. Clin. Investig. 96, 1336–1350.
Ren, K.W., Wu, J., Yan, F., Zhang, Y., Ju, H.X., 2015. Biosens. Bioelectron. 66, 345–349.
Ruslinda, A.R., Penmatsa, V., Ishii, Y., Tajima, S., Kawarada, H., 2012. Analyst 137, 1692–1697.
Tai, Z.X., Yan, X.B., Xue, Q.J., 2012. J. Power Sources 213, 350–357.
Vasudev, A., Kaushik, A., Bhansali, S., 2013. Biosens. Bioelectron. 39, 300–305.
Voiry, D., Yamaguchi, H., Li, J., Silva, R., Alves, D.C.B., Fujita, T., Chen, M., Asefa, T., Shenoy, V.B., Eda, G., Chhowalla, M., 2013. Nat. Mater. 12, 850–855.
Wang, J., Li, J., Baca, A.J., Hu, J., Zhou, F., Yan, W., Pang, D.W., 2003. Anal. Chem. 75, 3941–3945.
Wang, J., Meng, W.Y., Zheng, X.F., Liu, S.L., Li, G.X., 2009. Biosens. Bioelectron. 24, 1598–1602.
Wang, P., Song, Y.H., Zhao, Y.J., Fan, A.P., 2013. Talanta 103, 392–397.
Wu, Z., Tang, L.J., Zhang, X.B., Jiang, J.H., Tan, W., 2011. ACS Nano 5, 7696–7699.
Yang, Y.C., Li, C., Yin, L., Liu, M.Y., Wang, Z.X., Shu, Y.Q., Li, G.X., 2014. ACS Appl. Mater. Interfaces 6, 7579–7584.
Yin, Z.Y., Li, H., Li, H., Jiang, L., Shi, Y.M., Sun, Y.H., Lu, G., Zhang, Q., Chen, X.D., Zhang, H., 2012. ACS Nano 6, 74–80.
Zhang, H.Q., Li, X.F., Le, X.C., 2009. Anal. Chem. 81, 7795–7800.
Zhang, J.J., Cao, J.T., Shi, G.F., Huang, K.J., Liu, Y.M., Ren, S.W., 2015. Talanta 132, 65–71.
Zhu, X.L., Zhang, H.H., Feng, C., Ye, Z.H., Li, G.X., 2014. RSC Adv. 4, 2421–2426.
Zhu, Y., Hu, H., Li, W.C., Zhang, X., 2006. J. Power Sources 162, 738–742.